Fully reversible hydrogen absorption and desorption reactions with Sc(Al$_{1-x}$Mg$_x$), $x=$0.0, 0.15, 0.20

Martin Sahlberg [a],*, Claudia Zlotea [b], Michel Latroche [b], Yvonne Andersson [a]

[a] *Department of Materials Chemistry, The Ångström Laboratory, Uppsala University, Box 538, SE-751 21 Uppsala, Sweden*
[b] *Institut de Chimie et des Matériaux—Paris Est, CNRS UMR 7182, 94320 Thiais, France*

A R T I C L E   I N F O

A B S T R A C T

The hydrogen storage properties of Sc(Al$_{1-x}$Mg$_x$), $x=$0.0, 0.15, 0.20, have been studied by X-ray powder diffraction, thermal desorption spectroscopy, pressure-composition-isotherms and scanning electron microscopy techniques. Hydrogen is absorbed from the gas phase at 70 kPa and 400 °C under the formation of ScH$_2$ and aluminium with magnesium in solid solution. The reaction is fully reversible in vacuum at 500 °C and shows the hydrogenation–disproportionation–desorption-recombination (HDDR) behaviour. The activation energy of desorption was determined by the Kissinger method to 185 kJ/mol. The material is stable up to at least six absorption–desorption cycles and there is no change in particle size during cycling.

© 2010 Elsevier Inc. All rights reserved.

1. Introduction

Light-metal hydrides are today the most preferable hydrogen storage materials to meet all targets set by industry for mobile applications. Magnesium- and aluminium-based materials for hydrogen storage have been extensively studied during the last 40 years [1–3]. There are many advantages of magnesium hydride, such as high gravimetric and volumetric hydrogen contents, abundance on earth and low cost. However, the kinetic properties are unfavourable for rapid hydrogen absorption and desorption and the magnesium hydride is thermodynamically very stable. Alloying with other elements has been shown to improve the thermodynamic properties and the kinetics [4,5]. The lightest rare earth-like metal, scandium, reacts with hydrogen gas and forms ScH$_2$ with a high energy of formation 200 kJ/mol and significant hydrogen content 4.3 wt% [6,7].

Previous studies of hydrogen reactions with Sc–Mg and Sc–Al compounds [8–12] have shown that Sc$_2$Al and Mg$_{0.65}$Sc$_{0.35}$ absorb large amounts of hydrogen. However, no hydrogenation reversibility could be obtained for hydrogenated Sc$_2$Al and hydrogenated Mg$_{0.65}$Sc$_{0.35}$ was only partly dehydrogenated. Recently it was found by *in situ* synchrotron radiation X-ray diffraction, neutron diffraction and quantum mechanical calculations, that ScAl$_{0.8}$Mg$_{0.2}$ [13] absorbed and desorbed hydrogen reversibly. In a hydrogen atmosphere at 400 °C the CsCl-type structure ScAl$_{0.8}$Mg$_{0.2}$ decomposed to ScH$_2$ and Al(Mg). This reaction was fully reversible in vacuum at

500 °C. The maximum hydrogen storage capacity obtained was 2.7 wt%.

In the present study the hydrogen absorption and desorption properties of Sc(Al$_{1-x}$Mg$_x$), $x=$0.0, 0.15, 0.20 are reported from X-ray powder diffraction (XRD), thermal desorption spectroscopy (TDS) and scanning electron microscopy (SEM) investigations.

2. Experimental details

2.1. Sample preparation

Sc(Al$_{1-x}$Mg$_x$) with $x=$0.0, 0.15 and 0.20 were synthesised by direct reactions of the elements. Appropriate amounts of Mg (99.95%, Alfa Aesar), Sc (99.99%, Rare Earth products Ltd.) and Al (99.999%, Gränges SM), were sealed in a tantalum crucible under argon atmosphere and heated in an induction furnace at ~1100 °C in argon atmosphere (p(Ar)=40 kPa). After synthesis, all samples were grounded to powder in an agate mortar.

Hydrogenations of the mother compounds were performed using solid–gas reaction at a hydrogen pressure of 5 MPa and 420 °C. Prior to all hydrogenations, the reactor was evacuated and flushed with hydrogen several times to avoid oxide formation at elevated temperatures. No activation of the samples prior to hydrogenation absorption was needed.

2.2. Phase analysis and microstructural characterisation

Powder X-ray diffraction intensities were recorded on a Bruker D8 diffractometer with a Våntec position sensitive detector with 4°

opening using Cu$K\alpha_1$ radiation ($\lambda = 1.540598$ Å). Silicon was used as internal calibration standard. Unit cell axis refinements were performed using the programs CHECKCELL [14] and FULLPROF [15].

Microstructures and elemental analyses were obtained from a LEO 440 scanning electron microscope equipped with an EDAX energy dispersive detector. High resolution images were recorded with a LEO 1550 scanning electron microscope equipped with an in-lens detector. The samples were prepared by dispersing the powder material on carbon tape.

2.3. Thermal desorption spectroscopy

Thermal desorption spectroscopy (TDS) was performed in an ultra-high vacuum system equipped with a dynamic sampling mass spectrometer. Prior to the measurements the reactor was evacuated down to 10^{-6} Pa and flushed with nitrogen. The samples were heated with constant temperature rates (1–15 °C/min) and the partial pressures of hydrogen were recorded. The activation energy was determined using the Kissinger method [16]. The system was calibrated by desorbing a known standard hydride (TiH$_2$, Alfa Aesar) at different heating rates and different amounts.

2.4. Cycling

Absorption–desorption cycling were performed in a furnace system in the pressure range from ultra-high vacuum to a hydrogen pressure of 100 kPa. The samples were first hydrogenated *ex situ* at 5 MPa and 420 °C, and thereafter desorbed in UHV and rehydrogenated at 70 kPa and 400 °C. After five desorption–rehydrogenation cycles, TDS was performed on the samples for the sixth desorption. A small exposure to air during loading was unavoidable in the TDS experimental setup.

2.5. Pressure-composition-isotherms and kinetic isothermal measurements

The pressure-composition-isotherm (PCI) measurements were performed on the ScAl in powder form using the SETARAM PCTPRO volumetric instrument. The absorption isotherm at 385 °C (± 1) was recorded by stepwise increase of hydrogen pressure. The absorption kinetics is very slow and the equilibrium time is set to maximum 10 h.

The isothermal kinetic measurements were performed on powder samples using the SETARAM PCTPRO volumetric device. Absorption isothermal measurements were carried out at 400 °C (± 1) under hydrogen pressures between 0.15 and 4.4 MPa. Desorption was performed under dynamic vacuum at 530 °C (1 h). The hydrogen sorption performances were repeatable under similar pressure and temperature conditions.

3. Results and discussion

According to the X-ray powder diffraction profiles shown in Fig. 1, all mother compounds crystallised in the cubic CsCl-type structure. The unit cell parameter varied with the magnesium content in accordance to Vegard's law (see Fig. 1). The refined unit cell parameters were 3.383(3), 3.399(1) and 3.404(1) Å for $x=0.0$, 0.15 and 0.20, respectively.

The hydrogenated samples contained two phases, ScH$_2$ and aluminium with magnesium in solid solution [13]. ScH$_2$ crystallised in the CaF$_2$-type structure with the unit cell parameter 4.777(1) Å in agreement with previously reported data, $a=4.7832(4)$ Å [7]. Due to severe overlaps in the Bragg positions of ScH$_2$ and Al(Mg) the programme FULLPROF was used to refine the unit cell axis of ScH$_2$ and Al(Mg). The unit cell of Al(Mg) was

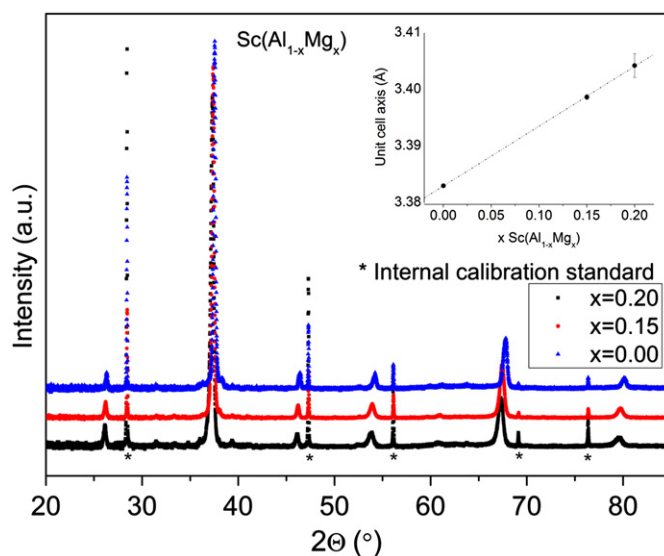**Fig. 1.** XRD pattern of Sc(Al$_{1-x}$Mg$_x$). From the top: $x=0$, 0.15, 0.20. Silicon is internal calibration standard. The inset shows the unit cell parameter as a function of the magnesium content.
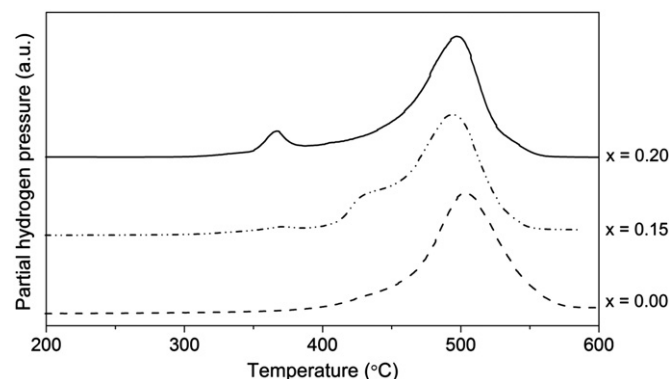

Fig. 2. Thermal desorption spectra of hydrogenated Sc(Al$_{1-x}$Mg$_x$) for $x=0$, 0.15 and 0.20 with the heating rate 5 °C/min. The thermal desorption spectra were recorded after the first absorption cycle.

refined to 4.106(2) Å ($x=0.20$). This value is, however, uncertain because of both the overlap and the large broadening of the peaks. For Al(Mg) in hydrogenated Sc(Al$_{1-x}$Mg$_x$) with $x=0.0$ and 0.15 the uncertainties in the Bragg peak positions were too large to obtain a value of the unit cell parameter. The very broad diffraction peaks indicated that the grains of the hydrogenated sample are very small.

3.1. Thermal desorption spectroscopy

TDS was performed on the hydrogenated compounds. The hydrogen desorption starts at ∼300 °C, and the maximum of temperature desorption (T_m) is ∼500 °C. As seen in Fig. 2, for $x < 0.20$ there was one large peak at ∼500 °C and for $x=0.20$ there were two peaks, a small peak at ∼365 °C and a large peak at ∼500 °C. The small peak at ∼365 °C probably originates from small amounts of amorphous MgH$_2$, since the maximum solid solubility of magnesium in aluminium is ∼18 at% [17].

The activation energy of hydrogen desorption was determined by the Kissinger analysis (Fig. 3). The activation energy was calculated for the reaction:
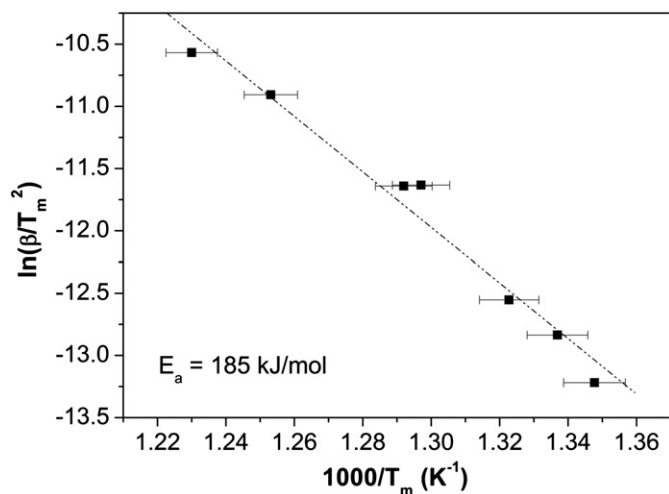
$$ScH_2 + Al_{0.8}Mg_{0.2} \rightarrow ScAl_{0.8}Mg_{0.2} + H_2$$
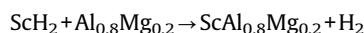
Fig. 3. Kissinger plot for the large desorption peak of hydrogenated Sc(Al$_{1-x}$Mg$_x$), $x=0.20$. The error bars indicate an estimated error of ± 5 °C.

The activation energy for ScAl$_{0.8}$Mg$_{0.2}$ was 139 kJ/mol for the small peak and 185 kJ/mol for the main peak. Both T_m and the activation energy for the small peak agreed well with the results of Han et al. [18] on the desorption of MgH$_2$ (142 kJ/mol). The activation energy of the main peak (185 kJ/mol) is quite high, no value of the activation energy of desorption for pure ScH$_2$ has been reported to our knowledge, but the corresponding value for YH$_2$ is 272 kJ/mol [19]. The high kinetic barrier of scandium hydride has previously been reported to hamper reactions that are thermodynamically favourable [20].

A comparison of the desorption temperature of ScH$_2$ [21] and hydrogenated Sc(Al$_{1-x}$Mg$_x$), 960 and 500 °C, respectively, revealed that aluminium and magnesium destabilised the scandium hydride. The destabilisation of scandium hydride by aluminium and magnesium is in good agreement with our previous calculations on ScAl$_{0.8}$Mg$_{0.2}$ [13]. Similar destabilisation has earlier been observed for hydrogen absorption/desorption reactions with YMgGa, where the formed stable yttrium dihydride was destabilised by gallium [22].

3.2. Reversibility

XRD patterns of the mother compounds Sc(Al$_{1-x}$Mg$_x$) $x=0.0$, 0.15, 0.20, hydrogenated and desorbed samples showed that the reactions with hydrogen were fully reversible. The diffraction profiles for Sc(Al$_{1-x}$Mg$_x$), $x=0.20$, are shown in Fig. 4. All hydrogen was desorbed and the mother compound was recovered. These compounds adopted the hydrogenation-disproportionation-desorption-recombination (HDDR) behaviour, commonly seen in Nd–Fe–B permanent magnets [23]. These results are in contrast to other studies of hydrogen storage in Sc–Al and Sc–Mg compounds where a full reversibility of hydrogen absorption/desorption have not been observed [9–12].

3.3. Cycling

Six absorption–desorption cycles were performed to evaluate the cycling stability of the material, for $x=0$. Fig. 5 shows the TDS spectra from the first and sixth desorption cycle. The temperature of maximum desorption is increased about 15 °C by cycling the material. This was unexpected since it is more common that the temperature of maximum desorption is lowered upon cycling [24]. The presence of small amounts of oxygen could not be avoided
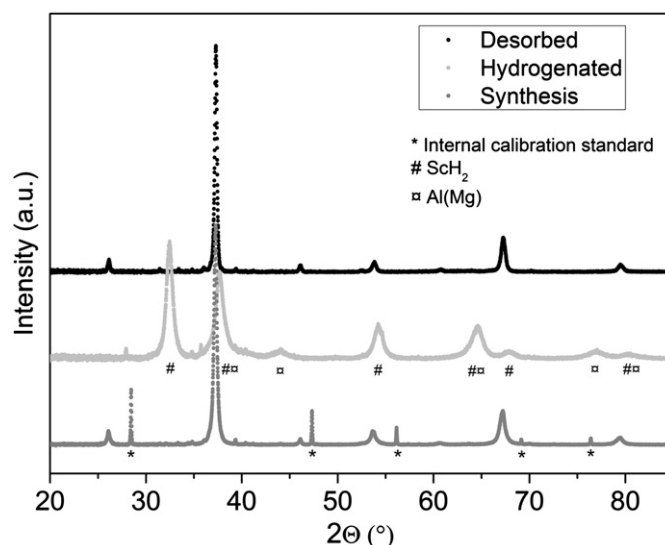

Fig. 4. XRD pattern of the mother compound Sc(Al$_{1-x}$Mg$_x$), $x=0.20$ (lower), hydrogenated sample (middle) and the desorbed sample (upper).

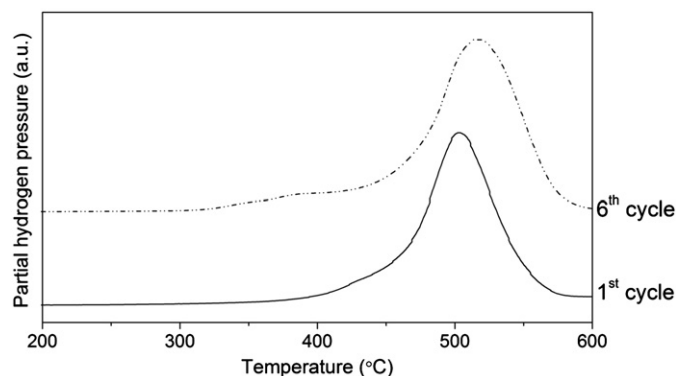**Fig. 5.** TDS spectra, of Sc(Al$_{1-x}$Mg$_x$) for $x=0$, recorded during the first and sixth desorption cycle.

during the experiments. The XRD patterns showed that small amounts of Sc$_2$O$_3$ were formed during cycling.

3.4. Microstructural characterisation

The SEM investigations show no change in particle size during cycling (Fig. 6). The overall compositions of ScAl$_{0.8}$Mg$_{0.2}$ and ScAl are confirmed by EDS, as shown in Fig. 6a–c.

The fact that the particle size did not change during hydrogen uptake and release was unanticipated as the HDDR behaviour commonly reduces the particle size of the material [23]. The constant particle size could explain the small changes of the maximum desorption temperature with cycling.

3.5. Pressure-composition-isotherms and kinetic isothermal measurements

The PCI curve recorded at 385 °C is displayed in Fig. 7. The shape of the PCI at very low pressures might indicate the formation of scandium hydride, which is in agreement with previous studies of ScH$_2$ formation at hydrogen pressures below 1 Pa (0.01 mbar) at 600 °C [25]. The maximum hydrogen uptake is 1.3 H/f.u., which is lower than the maximum theoretical capacity of 2 H/f.u. corresponding to the complete reaction: ScAl+H$_2$→ScH$_2$+Al. However,
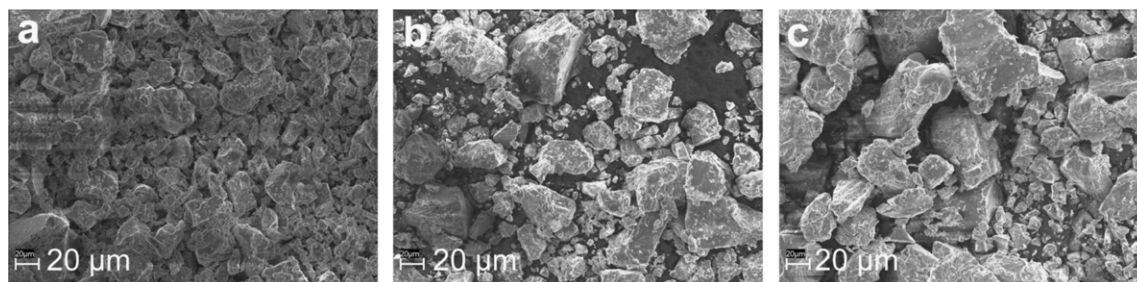
Fig. 6. SEM images: (a) hydrogenated sample $Sc(Al_{1-x}Mg_x)$, $x=0.20$, (b) Desorbed $Sc(Al_{1-x}Mg_x)$, $x=0.20$, (c) hydrogenated sample after six cycles $Sc(Al_{1-x}Mg_x)$, $x=0.0$. Magnification $1000\times$ for all images.
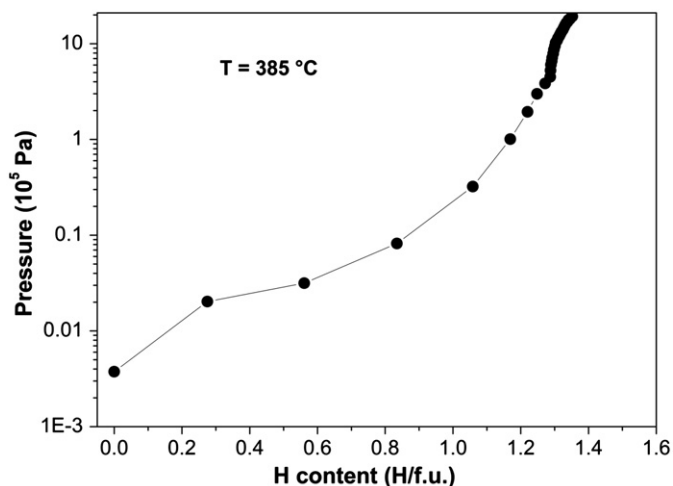

Fig. 7. Pressure-composition-isotherm of $Sc(Al_{1-x}Mg_x)$ for $x=0$, at 385 °C.
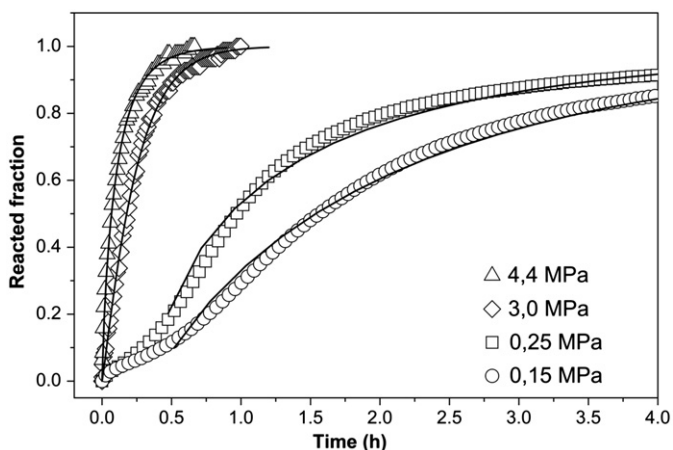
Fig. 8. Hydrogen absorption kinetics (symbols) for $Sc(Al_{1-x}Mg_x)$, $x=0.20$, at 400 °C under different hydrogen pressures together with the refined curves (lines).

the absorption kinetics are very slow at very low pressures and the hydrogenation might be uncompleted under this temperature and pressure conditions. This could explain the shape of the PCI at very low pressure and the lower hydrogen absorption capacity. Small amounts of $ScAl_2$ were formed during these measurements.

Fig. 8 shows the absorption kinetics recorded at 400 °C under different hydrogen pressures together with the refined curves on the basis of the Johnson-Mehl-Avrami (JMA) Equation [26]:

$$y(t) = 1 - \exp(-K(t-s)^n)$$

where y is the volume fraction of the reacted material, k is the kinetic parameter, t is the time variable, s is the incubation period and n is the Avrami exponent, which is characteristic of the growth mechanism.

The hydrogen absorption reaction follows several steps: dissociation of the hydrogen molecules to hydrogen atoms, surface penetration and diffusion of atomic hydrogen through the hydride layer, nucleation and growth of the hydride phase, where the slowest process is rate limiting.

The rate-limiting step of hydrogen absorption was determined from the Avrami n exponent [26]. This parameter was determined to values between 0.7 and 1.1 by JMA refinement of the kinetic curves (with the confidence factor of the fit $R=0.99$). These values correspond to fast nucleation with constant nuclei number and growth that is controlled by either one or two dimensional diffusion or one dimensional interface process [26–28]. However, a clear depiction of the nucleation and growth mechanism cannot by drawn from the sole value of the Avrami exponent. The incubation time was shown to decrease with the applied hydrogen pressure in agreement with the increase of the driving force, which is assumed to be proportional to $1-P/P_{eq}$ or $1-\sqrt{P/P_{eq}}$ [28], where P_{eq} is below 1 Pa at 400 °C).

The kinetic measurements showed that the sample was fully reacted after $\sim$1.0 h at 4.4 MPa and 400 °C, see Fig. 8.

4. Summary and conclusion

Hydrogen storage properties of $Sc(Al_{1-x}Mg_x)$ have been investigated for $x=0.0$, 0.15, 0.20. These compounds absorb hydrogen by decomposing into ScH_2 and Al(Mg). The hydrogen reactions are fully reversible and the material showed HDDR behaviour. The activation energy for hydrogen desorption was investigated with TDS and determined to 185 kJ/mol. The material is stable up to at least six absorption–desorption cycles and there is no change in particle size during cycling.

References

[1] B. Sakintuna, F. Lamari-Darkrim, M. Hirscher, Int. J. Hydrogen Energy 32 (2007) 1121.
[2] L. Schlapbach, A. Zuttel, Nature 414 (2001) 353.
[3] P. Selvam, B. Viswanathan, C.S. Swamy, V. Srinivasan., Int. J. Hydrogen Energy 11 (1986) 169.
[4] J.J. Reilly, R.H. Wiswall, Inorg. Chem. 6 (1967) 2220.
[5] J.J. Reilly, R.H. Wiswall, Inorg. Chem. 7 (1968) 2254.
[6] M.L. Lieberman, P.G. Wahlbeck, J. Phys. Chem. 69 (1965) 3514.

[7] J.C. McGuire, C.P. Kempter, J. Chem. Phys. 33 (1960) 1584.

[8] M.M. Antonova, V.B. Chernogorenko, Russ. J. Appl. Chem. 74 (2001) 396.

[9] G.S. Burkhanov, N.B. Kol'chugina, O.D. Chistyakov, V.N. Verbetsky, A.A. Salamova, E.Y. Andreeva, E.S. Volkova, Inorg. Mater. 42 (2006) 491.

[10] W.P. Kalisvaart, M. Latroche, F. Cuevas, P.H.L. Notten, J. Solid State Chem. 181 (2008) 1141.

[11] M. Latroche, P. Kalisvaart, P.H.L. Notten, J. Solid State Chem. 179 (2006) 3024.

[12] K.N. Semenenko, V.N. Verbetskii, T.K. Kurbanov, B.C. Alyev, A.A. Gasan-Zade, Zh. Neorg. Khim. 30 (1985) 1133.

[13] M. Sahlberg, P. Beran, T. Kollin Nielsen, Y. Cerenius, K. Kadas, M.P.J. Punkkinen, L. Vitos, O. Eriksson, T.R. Jensen, Y. Andersson, J. Solid State Chem. 182 (2009) 3113.

[14] J. Laguier, B. Bochu, Ecole Nationale Supérieure de Physique de Grenoble (INPG), France 2004.

[15] J. Rodríguez-Carvajal, FullProf Computer Program, version 3.5d 2004.

[16] H.E. Kissinger, Anal. Chem. 29 (1957) 1702.

[17] J.L. Murray, Bull. Alloy Phase Diagrams 3 (1982) 60.

[18] J.S. Han, M. Pezat, J.Y. Lee, J. Less-Common Met. 130 (1987) 395.

[19] J. Jung, J. Nucl. Mater. 49 (1974) 299.

[20] J. Purewal, S.-J. Hwang, R.C. Bowman, E. Ronnebro, B. Fultz, C. Ahn, J. Phys. Chem. 112 (2008) 8481.

[21] A.G. Aleksanyan, S.K. Dolukhanyan, V.S. Shekhtman, K.S. Harutyunyan, K.A. Abrahamyan, N.L. Mnatsakanyan, J. Alloys Compd. 356–357 (2003) 562.

[22] M. Sahlberg, C. Zlotea, P. Moretto, Y. Andersson, J. Solid State Chem. 182 (2009) 1833.

[23] I.R. Harris, P.J. McGuiness, J. Less-Common Met. 174 (1991) 1273.

[24] C. Zlotea, M. Sahlberg, S. Oezbilen, P. Moretto, Y. Andersson, Acta Mater. 56 (2008) 2421.

[25] F.D. Manchester, J.M. Pitre, J. Phase Equilibria 18 (1997) 194.

[26] P. Papon, J. Leblond, P. Meijer (Eds.), Springer-Verlag, 1999.

[27] A. Karty, J. Grunzweig-Genossar, P.S. Rudman, J. Appl. Phys. 50 (1979) 7200.

[28] J.F. Fernandez, C.R. Sanchez, J. Alloys Compd. 340 (2002) 189.